

**Polymer-free cubosomes for simultaneous bioimaging and photodynamic action of photosensitizers in melanoma skin cancer cells**

Urszula Bazylińska,<sup>a\*</sup> Julita Kulbacka,<sup>b</sup> Judith Schmidt,<sup>c</sup> Yeshayahu Talmon,<sup>c</sup> Sergio Murgia<sup>d\*</sup>

<sup>a</sup> Department of Organic and Pharmaceutical Technology, Faculty of Chemistry, Wrocław University of Science and Technology, Wybrzeże Wyspińskiego 27, 50-370 Wrocław, Poland.

<sup>b</sup> Department of Medical Biochemistry, Medical University of Wrocław, Chalubinskiego 10, 50-368 Wrocław, Poland.

<sup>c</sup> Department of Chemical Engineering, Technion-Israel Institute of Technology, Haifa 3200003, Israel

<sup>d</sup> Department of Chemical and Geological Sciences, University of Cagliari and CSGI, s.s. 554 bivio Sestu, I-09042 Monserrato (CA), Italy.

\* phone: +48 71 320 21 83; fax: +48 71 320 21 83; e-mail: urszula.bazylińska@pwr.edu.pl

\* phone: +39 0706754453; fax: +39 0706754388; e-mail: murgias@unica.it

**ABSTRACT**

We designed novel bioinspired monoolein-based cubic bicontinuous liquid crystalline dispersions (cubosomes) co-stabilized by phospholipids and propylene glycol. Their kinetic stability was evaluated by analysing the backscattering profiles upon ageing, and the most stable formulation was chosen as potential photosensitizers delivery vehicle for photodynamic therapy (PDT) of human skin melanoma cells. Morphological and topological features of such formulation alternatively loaded with Chlorin e6 or meso-Tetraphenylporphine-Mn(III) chloride photosensitizing dyes were investigated by cryo-TEM, DLS, and SAXS. Bioimaging studies demonstrated that Me45 and MeWo cell lines effectively internalized these cubosomes

formulations. Particularly, photodynamic activity experiments proved both the very low cytotoxicity of the cubosomes formulation loaded with Chlorin e6 dye in the “dark” condition, and its significant cytotoxic effect after photoirradiation. The toxic effect recorded when the photosensitizer was encapsulated within the cubosomes was shown to be one order of magnitude higher than that caused by the free photosensitizer. This is the first report of biocompatible polymer-free cubosomes for potential application in both PDT and bioimaging of skin malignant melanoma.

**KEYWORDS** Cubosomes, phospholipids, polypropylene glycol, Chlorin e6, meso-Tetraphenylporphine-Mn(III) chloride, Me45 cells, MeWo cells.

## 1. INTRODUCTION

Most of therapeutic and diagnostic agents devoted to clinical use in anticancer therapy exhibit several drawbacks related to their poor solubility, rapid clearance, high toxicity, and low biocompatibility.<sup>1-3</sup> To overcome these limitations, tumour targeted nanoparticles of biological inspiration have been engineered for the simultaneous integration of drugs and imaging agents, with the aim of imparting maximum therapeutic effect at specific places in the body, while reducing side-effects.<sup>3,4</sup> One type of such nanoparticles are known as cubosomes, typically formulated exploiting the natural tendency of some lipids to self-aggregate in water forming reverse cubic bicontinuous liquid crystalline structures. Since they can be simultaneously loaded with therapeutically active molecules and imaging agents, numerous investigations proved cubosomes useful for biomedical applications,<sup>5-8</sup> and recent studies evidenced they can be safely administered intravenously for *in vivo* fluorescent life-time analysis and for near-infrared fluorescence (NIRF) / magnetic resonance imaging (MRI) dual modality imaging study.<sup>9,10</sup> Cubosomes possess an inner nanostructure comprising a lipid bilayer arranged in three dimensions to form two continuous, nonintersecting water channels. To avoid phase separation, their stabilization in water is basically achieved by addition of polymeric tri-block non-ionic emulsifiers selected from the Pluronic group.<sup>6,8,11</sup>

Interestingly, by adding hydrophobic molecules the inner structure of cubosomes can be switched from cubic bicontinuous to reverse hexagonal thus originating the so-called hexosomes. Similarly to cubosomes, also these nanoparticles were investigated as biomedical tools and several *in vivo* evaluation studies have recently appeared.

It deserves here noticing that, the clinical application of Pluronics can be limited due to their potential cytotoxicity at higher concentrations, poor tissue-adhesion properties, and/or poor biodegradability.<sup>12,13</sup> Thus, the possibility of reducing the toxic impact at biological level of cubosomes was here explored by replacing Pluronic with the more biocompatible phospholipids. Phospholipids, as main components of human cell membranes, play important roles in protection and transport of cellular constituents, showing excellent biocompatibility.<sup>14,15</sup> Furthermore, due to their amphiphilic architecture, consisting of two hydrophobic fatty acid tails and a hydrophilic phosphate head joined together by an alcohol or glycerol molecule, these bio-inspired compounds are renowned for their self-assembly ability as well as emulsifying and wetting characteristics,<sup>16</sup> and often exploited to enhance hydrophilicity and compatibility of poorly water soluble molecules, including drugs. Self-assembly of natural (e.g., soybean or egg phosphatidylcholine) or synthetic phospholipids generates various supramolecular structures with unique properties useful in drug delivery and cancer imaging.<sup>16,17</sup>

When skin is the target of the drug to be delivered, the imperative challenge is overcoming the barrier represented by the *stratum corneum* (SC) to reach the subsequent skin layer, the viable epidermis. Indeed, SC consists of densely packed keratinocytes ordered in a characteristic “brick and mortar” configuration, acting as a phenomenal obstacle for transcutaneous administration of drugs. In time, nanoparticles have been developed to accomplish this task, liposomes denoting a lucid example of such development. Indeed, pristine liposomes show very little ability of penetrating the upper skin layer, thus remaining confined into the SC.<sup>18</sup> However, the importance in drug delivery through the skin of such nanoparticles was enormously enhanced, when their original nanostructure was modified leading to new generations of liposomes known as transferosomes, ethosomes, invasomes, and niosomes.<sup>18,19</sup> Remarkably, also cubosomes demonstrated their ability in delivering drugs through the SC, showing

performances in promoting the peptide vaccine penetration comparable to ethosomes, and superior to transferosomes. In the cases of both cubosomes and ethosomes the formulation permeability was supported by an addition of hydrotrope (polypropylene glycol or ethanol) molecules, acting as humectants to improve the SC hydration.<sup>18</sup>

Malignant melanoma is qualified as the most aggressive and life-threatening skin cancer, accounting for about 80% of deaths, and patients develop metastases with the 5-year survival rate being only 14%.<sup>20,21</sup> Currently available treatment options, such as chemotherapy, radiotherapy, and immunotherapy, are increasing, but the therapeutic outcome is still limited, because of the resistance of melanoma cells to these methods.<sup>21</sup> Therefore, there is still ample room for alternative treatment strategies, i.e., induction of tumour cells apoptosis by the generated reactive oxygen species (ROS) after photodynamic therapy (PDT) of cancer cells.<sup>22-</sup>

<sup>24</sup> PDT is a minimally invasive clinical procedure, which exploits photosensitive molecules called photosensitizer or photosensitizing agents, and a particular type of light. It is considered as an innovative method for resistant cancer cells treating. Furthermore, third generation of photosensitizers, e.g., cyanines, chlorines, or improved porphyrin-origin dyes encapsulated in novel colloidal nanocarriers, is of particular significance in designing anticancer therapeutics with both enhanced tumour selectivity and biocompatibility.<sup>24-26</sup>

The present contribution is focused on a newly engineered, polymer free, monoolein-based cubosomes formulation, whose stabilization is achieved by phospholipids and propylene glycol addition. Its physicochemical properties and *in vitro* biological impact on skin cancer cells when loaded with two types of third-generation photosensitizing agents (namely, Chlorin e6, Ce6, and meso-Tetraphenylporphine-Mn(III) chloride, TPP-Mn) are reported. To the best of our knowledge, this formulation is the first example of bioinspired cubic liquid crystalline dispersion for potential application in photodynamic therapy (PDT) and bioimaging of skin malignant melanoma.

## **2, MATERIALS AND METHODS**

### **2.1 Chemicals**

Phospholipids (Ph, fat free soybean phospholipids with 70% phosphatidylcholine and 7-10% phosphatidylethanolamine, Lipoid S75) were given by Lipoid GmbH, Germany. Monoolein (MO, 1-monooleoylglycerol, RYLO MG 19PHARMA, glycerol monooleate; 98.1 wt %) was a kind gift from Danisco A/S, DK-7200, Grinsted, Denmark. Propylene glycol (PG) was provided by Sigma Aldrich. Chlorin e6 (Ce6) and meso-Tetraphenylporphine-Mn(III) chloride (TPP-Mn) from Frontier Scientific were used as hydrophobic photosensitizers. Other reagents and solvents were of commercial grade, and were used as received. Water used for all experiments was doubly-distilled and purified by means of a Milli-Q purification system (Millipore, Bedford, MA).

### **2.2 Cubosomes preparation**

Cubosomes were prepared by dispersing the appropriate amount (see [Table 1](#)) of Phospholipid (Ph), monoolein (MO) and propylene glycol (PG) in water using an UP100H ultrasonic processor developed by Hielscher, cycle 0.9, amplitude 90 %, for about 10 min. Loaded cubosomes were obtained by dispersing the photosensitizer (PS, Ce6 or TPP-Mn) in the melted Ph + MO + PG with the help of an ultrasonic bath before dispersion in water. The total sample volume was 4 mL.

### **2.3 Cubosomes size and surface charge (Dynamic Light Scattering, DLS)**

The nanocarrier size distribution (i.e., the mean hydrodynamic diameter,  $D_H$ ) and polydispersity index (PdI) were determined by dynamic light scattering (DLS) using a Nano Series Zetasizer from Malvern Instruments, with a detection angle of  $173^\circ$  in optically homogeneous square polystyrene cells. All the measurements were performed at 25 °C. Each value was obtained as

an average of three runs with at least 10 measurements.  $\zeta$ -potential of the obtained cubosomes was measured by the microelectrophoretic method by the Malvern Zetasizer Nano ZS apparatus. Each value was obtained as an average of three subsequent runs of the instrument, with at least 20 measurements. All samples were diluted doubly-distilled water in the ratio 1:50 before  $D_H$  and  $\zeta$ -potential measurements. The DTS (Nano) program was used for data evaluation.

## **2.4 Cubosomes nanostructure (small-angle x-ray scattering, SAXS)**

SAXS curves were recorded with a S3-MICRO SWAXS camera system (HECUS x-ray Systems, Graz, Austria). A GeniX x-ray generator, working at 50 kV and 1 mA, provided Cu  $K\alpha$  radiation of wavelength 1.542 Å. A 1D-PSD-50 M system (HECUS x-ray Systems, Graz, Austria) with 1024 channels, 54.0  $\mu\text{m}$  wide, was used for detection of scattered x-rays in the small-angle region. The working  $q$  range ( $\text{\AA}^{-1}$ ) was  $0.003 \leq q \leq 0.6$ , where  $q = 4\pi\sin(\theta)\lambda^{-1}$  is the scattering wave vector. Thin-walled 2 mm glass capillaries were filled with the cubosomes dispersions. The diffraction patterns of cubosomes were recorded for 3 h. The lattice parameter  $a$  of the cubic phases was obtained using the equation  $a = d(h^2 + k^2 + l^2)^{1/2}$  from linear fits of the plots of  $1/d$  versus  $(h^2 + k^2 + l^2)^{1/2}$ , where  $d = 2\pi/q$  and  $h$ ,  $k$ , and  $l$  are the Miller indices. Water channel radii were calculated using the equation  $R_w = [(A_0/2\pi\chi)^{1/2}a] - L$ , where  $L$  is the lipid length value (17 Å),  $a$  is the lattice parameter obtained from the SAXS analysis, and  $A_0$  and  $\chi$  are the surface area and the Euler characteristic of the infinite periodic minimal surface geometries ( $Pn3m$ ,  $A_0 = 1.919$ ,  $\chi = -2$ ;  $Im3m$ ,  $A_0 = 2.345$ ,  $\chi = -4$ ).

## **2.5 Cubosomes morphology (cryogenic transmission electron microscopy, cryo-TEM)**

Cryo-TEM experiments were performed to image the cubosomes nanoparticles. Specimens were vitrified in a controlled environment vitrification system (CEVS) at 25 °C and 100 % relative humidity. A drop (about 3  $\mu\text{L}$ ) of the sample was placed on a perforated carbon film-

coated copper grid, blotted with filter paper, and plunged into liquid ethane at its freezing point. Such specimens were then transferred to a 626 Gatan cryo-holder and observed at 200 kV acceleration voltage in an FEI Talos 200C high-resolution transmission electron microscope at about  $-175\text{ }^{\circ}\text{C}$ , in the low-dose imaging mode to minimize electron-beam radiation-damage. Images were digitally recorded with either with an FEI Ceta 16M 16 megapixel CCD camera or with an FEI Falcon II direct-imaging 16 megapixel camera.

## **2.6 Photosensitizers encapsulation efficiency (UV-Vis spectroscopy)**

To evaluate the photosensitizers (PSs) encapsulation efficiency (EE%) in the different cubosomes formulations investigated, UV-vis absorbance measurements were performed following dialysis of the non-encapsulated PS molecules, following the previously described purification method.<sup>8,27</sup> Measurements were performed using a Metertech SP8001 spectrophotometer with 1 cm path thermostated length quartz cell. The cargo content was quantified at  $\lambda_{\text{Ce6}} = 405\text{ nm}$  and  $\lambda_{\text{TPP-Mn}} = 470\text{ nm}$  after the disruption of cubosomes with THF:water (3:1). The PS encapsulation efficacy was quantified as follows:  $\text{EE (\%)} = (\text{weight of the PS in cubosomes})/(\text{weight of the feeding PS}) \times 100\%$ .

## **2.7 Nanocarrier kinetic stability (Backscattering profiles, BS)**

The long-term kinetic stability of the obtained cubosomes was studied with the TurbiScanLab Expert (Formulacion SA, France) by measuring the backscattering (BS) of pulsed near infrared light ( $\lambda = 880\text{ nm}$ ). The formulations were scanned in a cylindrical glass cell at  $25\text{ }^{\circ}\text{C}$ , while moving along the entire height of the cell, and BS profiles as a function of sample height were collected and analysed using the instrument software (Turbisoft version 2.0.0.33). The Turbiscan Stability Index (TSI) was calculated to determine the phospholipid and propylene

glycol efficiency in stabilizing the formulation, and to detect any destabilization phenomena in the samples versus ageing (up to 60 days), according to our previous studies.<sup>24,26</sup>

## **2.8 Human skin cancer cell culture**

Experiments concerning biological evaluation of the encapsulated cargo were performed on well characterized human skin cancer cell lines, i.e., malignant melanoma media cells derived from a lymph node metastasis of skin melanoma (Me45), and melanoma granular fibroblasts (MeWo). The Me45 cell line was obtained from the Oncology Centre Gliwice, where the line was derived from a 35-year-old woman's lymph node cells. The MeWo cell line was purchased from CLS (Cell Lines Service, Germany). The cell culture condition was applied as previously described.<sup>28</sup> In detail, the cells were cultured in culture flasks (25 cm<sup>3</sup>, Falcon) in DMEM (Sigma) with 2 mmol/l glutamine and 10 % fetal bovine serum (FBS, Bio Whittaker, Fetal Bovine Serum, South American origin). The cultures were incubated at 37 °C and in the presence of 5 % CO<sub>2</sub> humidified atmosphere. Cells intended for experiments were trypsinized (Trypsin-EDTA solution, T4049, Sigma-Aldrich), and then rinsed twice with PBS.

## **2.9 Bioimaging (Confocal laser scanning microscopy, CLSM)**

Intracellular internalization, localization and distribution of encapsulated photosensitizer delivered to the skin cancer cells were analysed using a FluoView FV1000 confocal laser scanning microscope (CLSM, Olympus). The images were recorded with a Plan-Apochromat 60x oil-immersion objective. After cultivation in standard conditions, the tumour Me45 or MeWo cells were seeded on microscopic cover slips placed in Petri dishes (35 mm, Nunc, Poland), and harvested for 24 h. In the next step the cells were incubated with PS-loaded cubosomes at  $2 \times 10^6$  M concentration of Ce6 or TPP-Mn. Moreover, the studied cells treated with the same concentration of free (unloaded) PS molecules were used as a positive control.

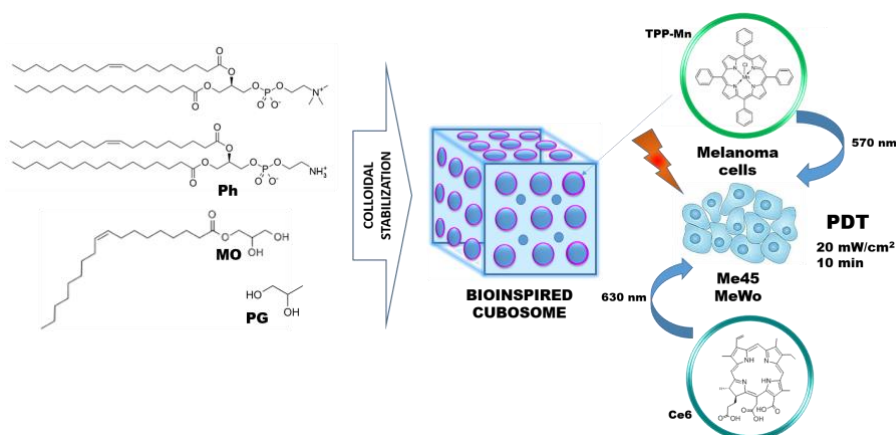
After 24 h incubation, the treated solution was removed, and the cover glasses were washed with PBS, fixed for 10 min in 4 % paraformaldehyde (PFA), and washed again with PBS. Slides were mounted in fluorescence mounting medium (DAKO), containing DAPI (4,6-diamidino-2-phenylindole) for nuclei staining. The preparations were stored in darkness at 4 °C, and then prepared for scanning according to the confocal laser scanning microscopy manual. Cell specimens were excited by He-Ne laser light ( $\lambda = 633$  nm for Ce6 and  $\lambda = 543$  for TPP-Mn) and diode laser light ( $\lambda = 405$  nm for DAPI).

### **2.10 Assay of *in vitro* photo-induced anticancer efficacy (MTT cell proliferation test)**

The *in vitro* anticancer activity of the studied cubosomes loaded with Ce6 or TPP-Mn at four different concentrations (1, 2, 5 and 10  $\mu$ M) after dilution in the culture media was tested in comparison with their free form using a MTT cell proliferation assay (Sigma), according to the manufacturer's protocol.<sup>26,29</sup> The cells were irradiated after 4 h of their cultivation for 10 min with a total light dose of 10 J/cm<sup>2</sup> using a lamp (OPTEL Opole, Fibre Illuminator, Poland) with polarized light filtered with barrier filters ( $\lambda_{\max}$  530–570 nm for TPP-Mn (III) Cl and  $\lambda_{\max}$  600–630 nm for Ce6). The energy fluency rate was 10 mW/cm<sup>2</sup> at the level of the cell monolayer. MTT assay for evaluation of PDT effectiveness was used after 24 h post irradiation. The cell viability in each group was expressed as a percentage of control (untreated with studied nanocarriers) skin cancer cells. The data were obtained by calculating the average of three experiments.

## **3. RESULTS AND DISCUSSION**

### **3.1 Physicochemical characteristics of cubosomes formulation**



**Scheme 1.** General strategy applied for the assembly of bioinspired cubosomes loaded by Ce6 or TPP-Mn photosensitizing dyes for photodynamic therapy (PDT).

The strategy used for the assembly of biocompatible cubosomes formulated by mixing phospholipids (Ph, used as stabilizer), monoolein (MO, the molecular building block of the cubosomes) and propylene glycol (PG, the hydrotrope) is presented in [Scheme 1](#). Samples composition was optimized for encapsulation of Ce6 or TPP-Mn photosensitizing dyes by varying the amount of PG in the range 0 to 1.00 wt %, while keeping constant the MO/Ph ratio (3.75/1.00) in a large excess of water (> 94 wt %). Five types of cubosomes dispersions (systems 1-5 in [Table 1](#)) were successfully formulated.

**Table 1.** Samples composition.

Sample	MO	Ph	PG	W
	Contents / wt %			
1	3.75	1.00	1.00	94.25
2	3.75	1.00	0.75	94.50
3	3.75	1.00	0.50	94.75
4	3.75	1.00	0.25	95.00

<b>5</b>	3.75	1.00	-	95.25
<b>6 (PS<sub>1</sub>)</b>	3.75	1.00	0.75	94.50
<b>7 (PS<sub>2</sub>)</b>	3.75	1.00	0.75	94.50

---

*MO*: monoolein, *Ph*: phospholipid, *PG*: propylene glycol,  
*W*: water, *PS<sub>1</sub>*: Ce6, *PS<sub>2</sub>*: TPP-Mn.

The mean diameter ( $D_H$ ), polydispersity index (PdI) and zeta ( $\zeta$ ) potential reported in [Table S1 \(Supporting Information\)](#) were assessed the day of cubosomes production, as well as after 21 days storage at room temperature in the dark. The mean particle sizes displayed an average size between 130 and 162 nm, PdI was found in the range 0.133-0.279, and negative  $\zeta$ -potential values of the surface charge were measured from -34 mV to -55 mV. Remarkably,  $\zeta$ -potential values recorded are in good agreement with literature data reported for stable delivery carriers designed for anticancer applications, since for any physically stable nanoparticles stabilized by combined electrostatic and steric repulsion forces, a zeta potential of  $\pm 20$  mV is required as minimum.<sup>30</sup> These results indicated that the PG molecules affected all recorded parameters, and showed that sample 2 (0.75 wt % of added PG) was the most promising candidate for hosting the photosensitizers, showing one of the most negative  $\zeta$ -potential, and the smaller average size and polydispersity index among the formulated systems. Results collected on the same samples after 21 days of storage strongly supported this choice, since sample 2 practically did not change with time. Therefore, sample 2 was loaded either with Ce6 or TPP-Mn photosensitizing dyes and further analysed by DLS, cryo-TEM, and SAXS.

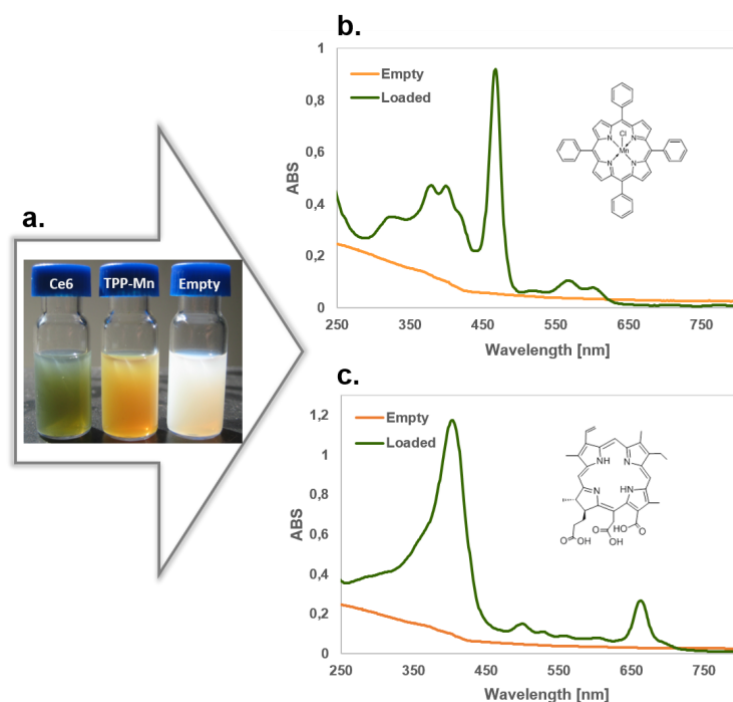


**Figure. 1.** Image (a) and UV–vis spectra of the obtained cubosomes loaded with TPP-Mn (b) and Ce6 (c) photosensitizers compared to the spectra of empty cubosomes.

UV–vis spectra of loaded and empty cubosomes are compared in [Figure 1](#). Particularly, both hydrophobic photosensitizing dyes were loaded with high encapsulation efficacy (EE% equal to 91 % and 97 % for TPP-Mn and Ce6, respectively). DLS experiments pointed out that encapsulation of (hydrophobic) photosensitizers within the cubosomes lipid matrix did not significantly modify size and surface charge of nanoparticles, the comparison with empty cubosomes (sample 2) showing only a slightly increased PDI value, more marked when cubosomes were loaded with Ce6. In [Figure 2](#) cryo-TEM gives images of samples 2, 6, and 7.

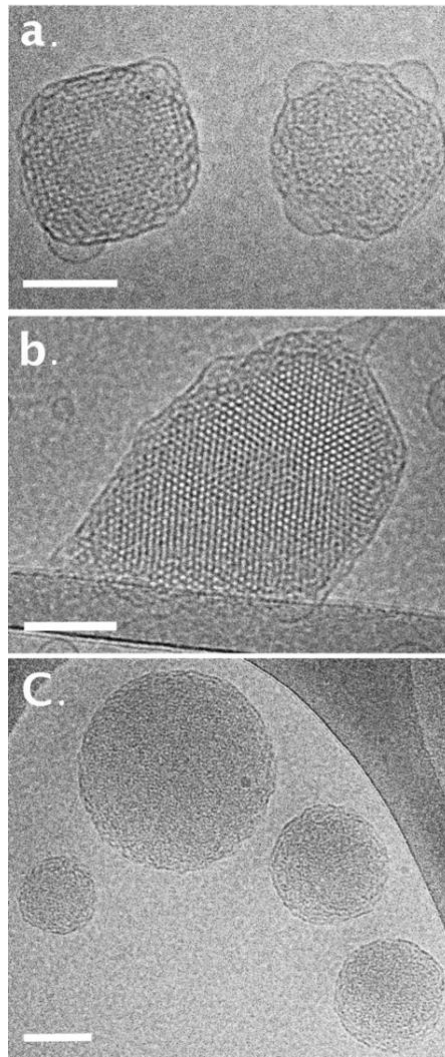


**Figure 2.** Cryo-TEM images of cubosomes empty (a) and loaded with TPP-Mn (b) and Ce6 (c) photosensitizers (respectively, samples 2, 6, and 7 in Table 1). Scale bars correspond to 100 nm.

All samples are characterized by the presence of spherical or quasi-spherical aggregates displaying a dense core and having size on the nanometer scale. However, only sample 2 and 6 clearly showed the classical arrangement of white spots alternate with the lipid matrix typical of reverse cubic bicontinuous phases. SAXS experiments were carried out to definitely establish the inner nanostructure of sample 2, 6, and 7. Particularly, the concurrence of two phases were detected from the analysis of the diffractograms shown in [Figure 3](#).

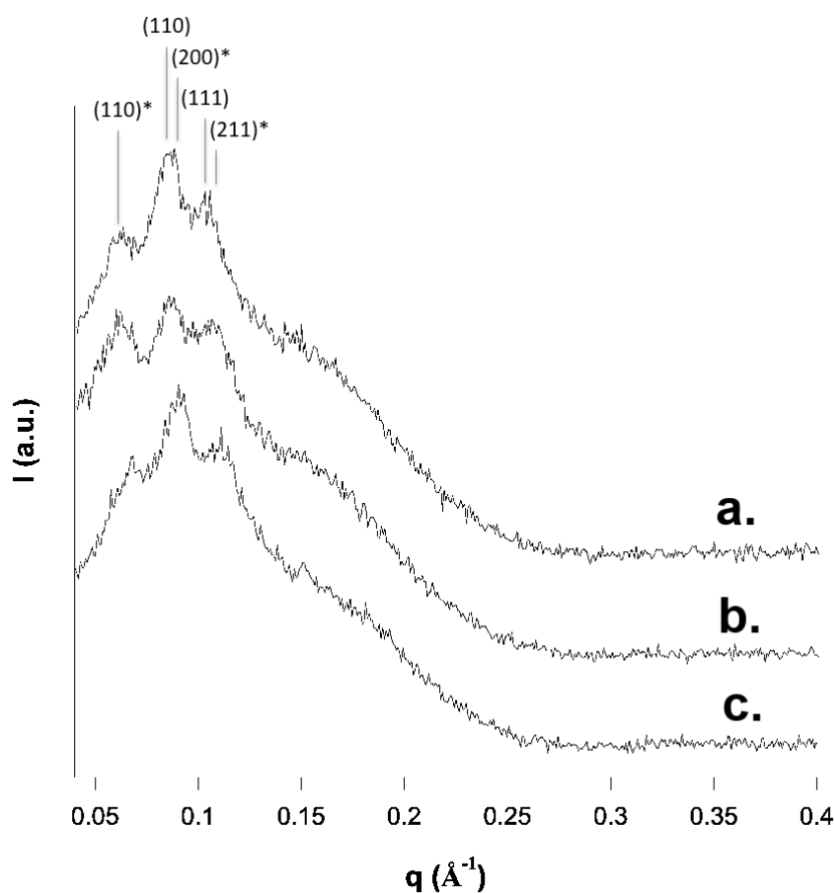


**Figure 3.** SAXS patterns of empty (a) and photosensitizer loaded, TPP-Mn (b), and Ce6 (c) cubosomes (respectively samples 2, 6, and 7 in Table 1). Reflections indicated by an asterisk refer to the Im3m phase.

Indeed, the presence of a double-diamond reverse bicontinuous cubic phase (belonging to Pn3m crystallographic space group) was indicated by two Bragg peaks with relative positions in a ratio of  $\sqrt{2}:\sqrt{3}$ , indexed as the (110) and (111) reflections. Moreover, the simultaneous presence of a primitive reverse bicontinuous cubic phase (belonging to the Im3m crystallographic space group) was indicated by three Bragg peaks with relative positions in a ratio of  $\sqrt{2}:\sqrt{4}:\sqrt{6}$ , respectively indexed as the (110), (200), and (211) reflections. Therefore, from SAXS experiments, all samples were definitely assessed as cubosome formulations, and structural parameters such as the lattice parameter (a) and the water channel radius ( $r_w$ ), were calculated and reported in [Table 2](#).

### 3.2 Kinetic stability evaluation by backscattering profiles

Turbiscan Lab Expert optical analyser instrument allows observing the sample progress in time by detecting different types of formulation instability, including the phenomena of flocculation, coalescence, sedimentation and creaming.<sup>26,31</sup> Thus, the turbidimetric method (opaque samples) was used to evaluate in detail the backscattering profiles of the cubosomes formulations (Figure 4), followed by evaluation of their Turbiscan Stability Indices (TSI) as a function of time (Table 2S in Supporting Information). The dynamics of the processes occurring in the formulations under investigation were determined after 21, 35 and 60 days of storage. Representative Turbiscan plots are shown in Figure 4 for samples 2 and 5. Here, the x-axis shows the different height (expressed in mm) of studied cubic dispersions in the measurement tube, while the y-axis corresponds to the percentage change of backscattering (BS) in relation to the initial state (the freshly prepared sample). From the plots presented in Figure 4a, we observe only small changes in BS of system 2 within a range of 10 % after 60 days of storage time, indicating that there is no evident particle growth or migration in solution, since rapid destabilization phenomena are characterized by a large separation between the curves in the middle (particle size increase because of flocculation), left side (sedimentation) or right side (creaming) of the recorded plots.<sup>31</sup> Differently, system 5 was clearly affected by creaming and flocculation destabilization phenomena.

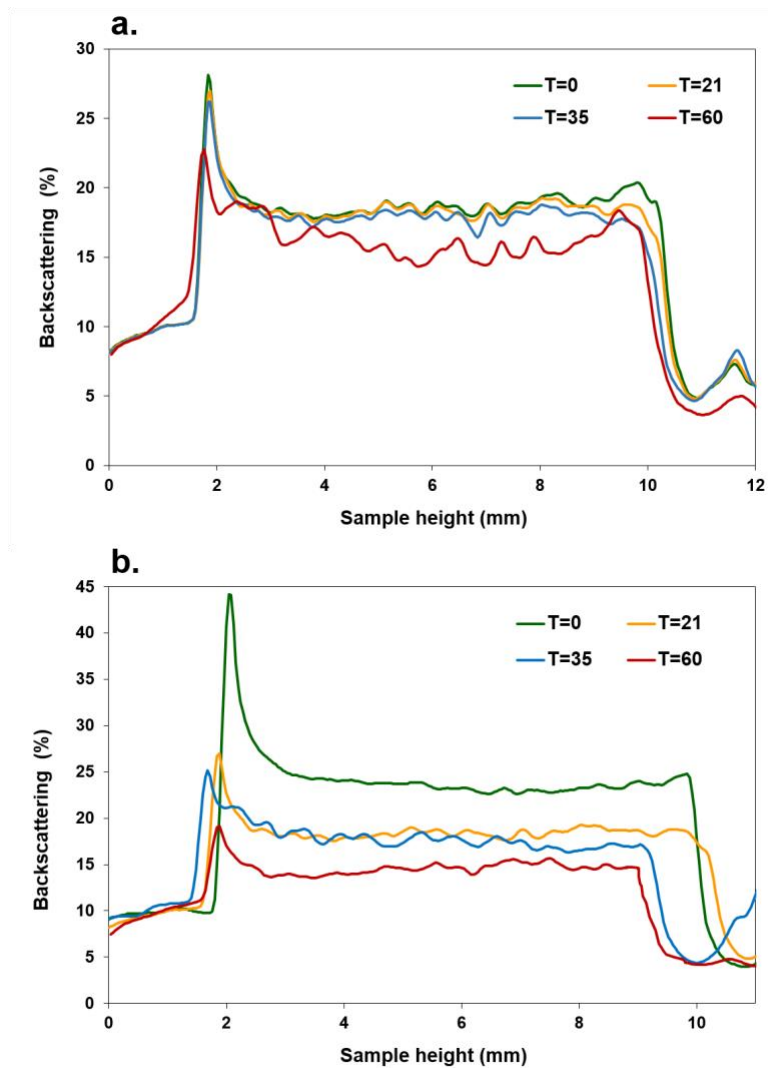


**Figure 4.** Backscattering (%) profiles of the obtained cubosomes as a function of sample height (mm) for samples 2 (a) and 5 (b). For description of the samples see Table 1.

These results correlate well with data obtained by DLS (Table S1 in SI), where increases in  $D_H$  (from 161 to 171 nm) and PDI (from 0.279 to 0.329) after 21 days were observed. These findings were also supported by the global stability-dependent TSI values of cubosomes as a function of time. As shown in Table S2 PG molecules, acting as a hydrotrope, affected the cubosomes kinetic stability. Accordingly, the sample without any addition of PG (sample 5) presents the poorest stability, since the higher the TSI value, the less stable will be the formulation.<sup>32</sup> With the addition of the hydrotrope sample stability increases up to its optimal concentration of 0.75

wt %. Such results are in good agreement with data reported in [Table 1](#). In literature, this phenomenon is explained as a transient stabilization of the formulation by hydrotropic molecules during the dispersion process obtained through homogenous distribution of the stabilising surfactant (the phospholipid mixture) on the cubosomes surface during the nucleation process.<sup>33</sup> As a consequence, the co-stabilized molecules lower the oil–water interfacial tension that favours the emulsification of monoolein in water, finally resulting in production of cubosomes without addition of the stabilising polymer (e.g. Pluronic). Nevertheless, with the increase of PG up to 1.00 wt% (sample 1) we observe a decrease of the sample stability. This is probably caused by a spontaneous association between excessive hydrophobic groups and phospholipid molecules, resulting in formation of other self-assembled nanostructures, e.g., vesicles.<sup>34</sup> Based on these results, the most favourable and long-lasting nanoformulation was selected for delivering Ce-6 or TPP-Mn (samples 6 and 7 from [Table 1](#)) to the skin cancer melanoma cells, since comparing the obtained TSI values ([Table S2](#)) we can claim that the encapsulation process only slightly affects the stability of the loaded cubosomes, proving the high pharmaceutical potential of these nanocarriers.

### **3.3 Bioimaging studies**

Given the peculiar composition, the proposed cubosomes formulations may have potential application in topical therapies of skin cancers. Indeed, monoolein, especially when formulated along with propylene glycol,<sup>35</sup> demonstrated pronounced properties as skin penetration enhancer.<sup>36</sup> Moreover, PG should act as a humectant weakening the intracellular SC lipid structure, and favouring the encapsulated molecules permeation through the skin.<sup>18</sup> Finally, the replacement of the Pluronic commonly used to stabilize these colloidal dispersions with the more biocompatible Ph should decrease the toxicity of the formulation, while enhancing its biodegradability and attracting further *in vivo* applications.

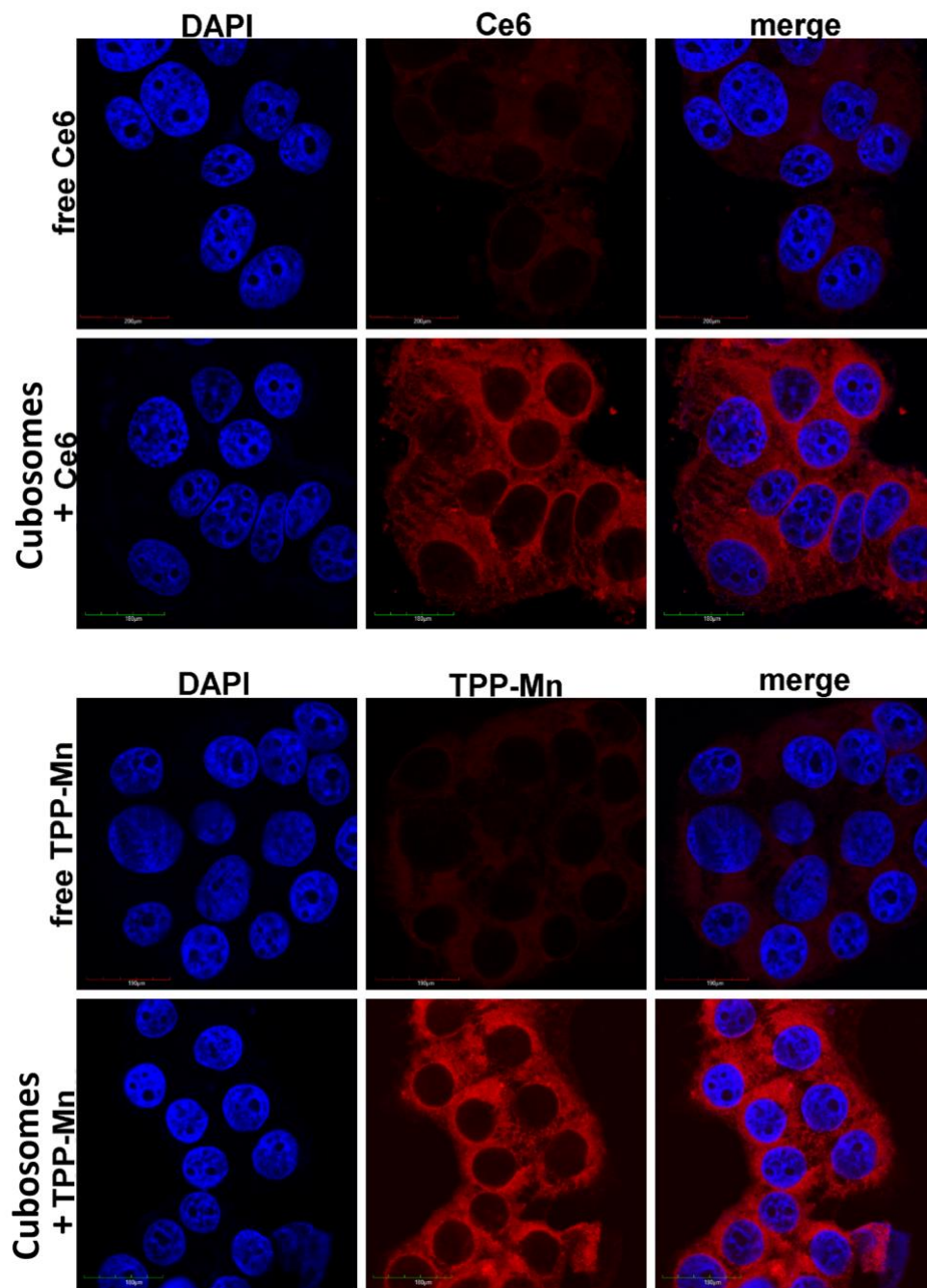


**Figure 5.** Intracellular distribution of Ce6 or TPP-Mn delivered with cubosomes to the MeWo melanoma cells (nuclei stained with DAPI in blue and PS signal in red).

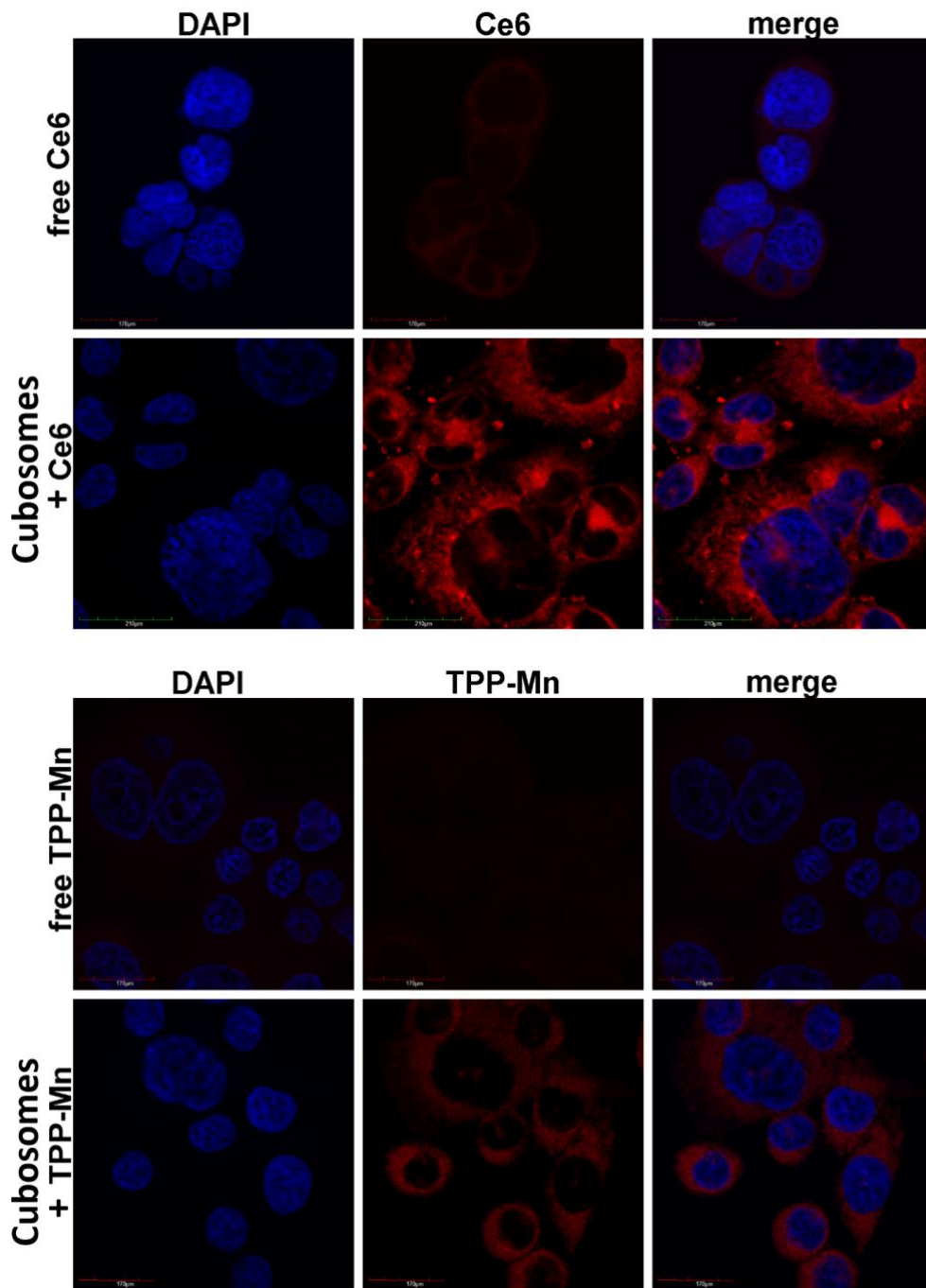


**Figure. 6.** Intracellular distribution of Ce6 or TPP-Mn delivered with cubosomes to the Me45 melanoma cells (nuclei stained with DAPI in blue and PS signal in red).

To explore the potential for skin cancer treatments, confocal laser scanning microscopy (CLSM) images were taken to record uptake and intracellular distribution of encapsulated and free (native) Ce6 and TPP-Mn molecules in the cell monolayer of microcultures of human

malignant skin melanoma cells (Figure 5 and Figure 6). Two human malignant melanoma media cell lines were selected as an *in vitro* model of skin derived malignancies, cells derived from a lymph node metastasis of skin melanoma (Me45), and melanoma granular fibroblasts (MeWo). Figure 5 and Figure 6 display the fluorescent images with 409 nm (DAPI), 543 nm (TPP-Mn), and 633 nm (Ce6) excitation, respectively, along with the overlay of both images. The cell nuclei were stained with 4',6-diamidino-2-phenylindole (DAPI, blue) and the PS fluorescence (Ce6 or TPP-Mn, red) in the cytoplasm could be clearly observed in both Me45 and MeWo cells, confirming that encapsulated cubosomes could be internalized by both skin cancer cells through endocytic process to emit fluorescence.<sup>37</sup> Although Me45 took up less effectively TPP-Mn than MeWo cell line, an enhanced cellular internalization, and a consequent stronger fluorescence signal, was detected for both photosensitizers, when they were encapsulated within cubosomes rather than when administered to cells in their free form. These results support the great potential of the proposed nanoparticles in PS delivering, skin cancer cell labelling and bioimaging.

### **3.4 Cytocompatibility and photodynamic activity**

Colloidal nanoparticles can be useful as photosensitizer delivery systems in PDT only if their “dark toxicity” is quite low, and significantly increases after photoirradiation.<sup>38</sup> Results presenting the cytocompatibility and photodynamic potential of the cubosomes loaded with Ce6 or TPP-Mn towards human melanoma (Me45 or MeWo) cells evaluated via methyl thiazolyltetrazolium (MTT) assay are shown in Figure 7. To compare the cytotoxic effect of the loaded photosensitizers in the absence of irradiation (dark cytotoxicity), four different concentrations of TPP-Mn or Ce6 were evaluated. Me45 cells viability was more than 50 % when the cells were incubated with both type of cubosomes in the final PS concentration of 1 or 2  $\mu$ M. In the case of MeWo, the cells were more resistant to the encapsulated Ce6 with the

non-toxic PS level of 5  $\mu\text{M}$ , indicating the good biocompatibility of the applied cubosomes. It should be noted, that free Ce6 molecules probably could not efficiently enter the melanoma cells and/or undergo aggregation in physiological conditions, since their “dark cytotoxicity” in the applied concentration range was quite low.<sup>19,25</sup>

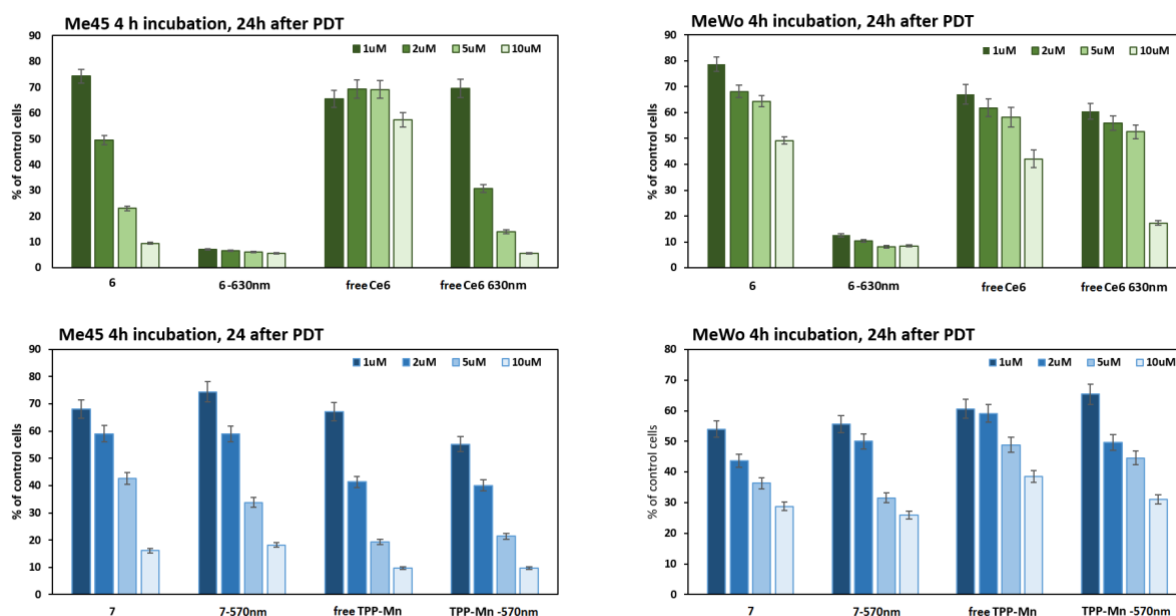


**Figure 7.** The effect of free and encapsulated PS (Ce6 or TPP-Mn) on the viability of Me45 or MeWo melanoma cells before and after photoirradiation - PDT.

This remark is supported by the poor fluorescence of the free Ce6 molecules observed in the skin cancer cells and presented before in Figure 5. Concerning the cubosomes formulation loaded with Ce6 at the smaller concentration used (1  $\mu\text{M}$ ) and administered to Me45 cells, it demonstrated excellent photodynamic properties, showing very low (if any) toxicity in the dark, and a provoking a huge reduction of cell viability (about 90 %) after irradiation. Remarkably, this formulation offered the same photodynamic performances of the free photosensitizer administered at a concentration one order of magnitude larger. Similar results were collected when administering Ce6 loaded cubosomes to MeWo cells. Thus, such formulation can be considered as biocompatible for the targeted cells, simultaneously enhancing the photosensitive

therapeutic effect of the light-activated Ce6. Conversely, the cubosomes loaded with TPP-Mn demonstrated only low photocytotoxicity on both melanoma cells, indicating the poor potential of such formulation in PDT. Nevertheless, the good fluorescent performances presented in CLSM internalization studies indicate that this dye as a good biomarker for cancer cells imaging.

#### **4. CONCLUSIONS**

We engineered polymer-free, monoolein cubosomes co-stabilized by a mixture of phospholipids (at least in principle, responsible for an improved formulation biocompatibility and biodegradability) and propylene glycol molecules, playing a dual role in our formulation, being at the same time a hydrotrope and a humectant. Particularly, we found that propylene glycol affected cubosome physicochemical properties, allowing the highest nanocarrier stability and the most favourable values of  $\zeta$ -potential (-54 mV), average size ( $D_H \sim 130$  nm) and narrow size distribution ( $PdI < 0.15$ ) when added as 0.75 wt % of the formulation. This sample was selected as the most promising candidate as carrier for the photosensitizing dyes. The bioimaging studies revealed the cytoplasmic localization of the encapsulated cargo in MeWo and Me45 melanoma cells, confirming the high potential of the obtained cubosomes in skin cancer diagnostics. We also showed the biocompatibility and high photodynamic activity of the encapsulated Ce6, proving over 90 % reduction of both MeWo and Me45 cells viability after irradiation and showing even greater photodynamic action than the free photosensitizer administered at concentration one order of magnitude higher.

As a whole, results present here will allow designing and developing a new generation of bioinspired drug delivery nanocarriers with a cubic structure for potential application in photodynamic therapy of melanoma skin cancer, extending the possibility to use the encapsulated Ce6 and TPP-Mn photosensitizers as candidates for effective bioimaging and maximum tumour damage via photoactivation.

## ACKNOWLEDGEMENTS

This work was supported by National Science Centre (Poland) within the framework of SONATA 8 programme (No.2014/15/D/ST4/00808). The cryo-TEM work was performed at the Technion Center for Electron Microscopy of Soft Matter, supported by the Technion Russell Berrie Nanotechnology Institute (RBNI). Dr. Valeria Meli is kindly thanked for some support during sample preparation.

## REFERENCES

- (1) Zhao, L.; Shen, G.; Ma, G.; Yan, X. Engineering and Delivery of Nanocolloids of Hydrophobic Drugs. *Adv. Colloid Interface Sci.* **2017**, DOI: 10.1016/j.cis.2017.04.008.
- (2) Su, Y.; Xie, Z.; Kim, G. B.; Dong, C.; Yang, J. Design Strategies and Applications of Circulating Cell-Mediated Drug Delivery Systems. *ACS Biomater. Sci. Eng.* **2015**, *1*, 201–217.
- (3) Sobot, D.; Mura, S.; Couvreur, P. How Can Nanomedicines Overcome Cellular-Based Anticancer Drug Resistance. *J. Mater. Chem. B* **2016**, *4*, 5078–5100.
- (4) Sheikhpour, M.; Barani, L.; Kasaeian, A. Biomimetics in Drug Delivery Systems: A Critical Review. *J. Control. Release* **2017**, *253*, 97–109.
- (5) Monduzzi, M.; Lampis, S.; Murgia, S.; Salis, A. From Self-Assembly Fundamental Knowledge to Nanomedicine Developments. *Adv. Colloid Interface Sci.* **2014**, *205*, 48–67.
- (6) Mulet, X.; Boyd, B. J.; Drummond C. J. Advances in Drug Delivery and Medical Imaging using Colloidal Lyotropic Liquid Crystalline Dispersions. *J. Colloid Interface Sci.* **2013**, *393*, 1-20.
- (7) Negrini, R.; Fong, W. K.; Boyd, B. J.; Mezzenga, R. pH Responsive Lyotropic Liquid Crystals and Their Potential Therapeutic Role in Cancer Treatments. *Chem. Commun.* **2015**, *51*, 6671–6674.

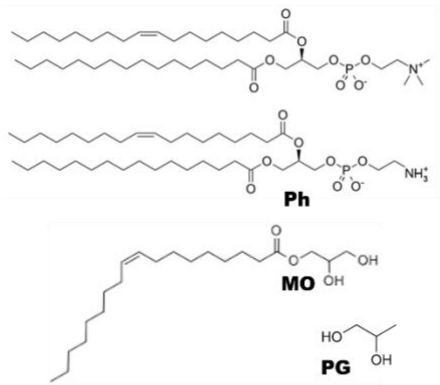
- (8) Meli, V.; Caltagirone, C.; Falchi, A. M.; Hyde, S. T.; Lippolis, V.; Monduzzi, M.; Obiols-Rabasa, M.; Rosa, A.; Schmidt, J.; Talmon Y.; Murgia, S. Docetaxel-Loaded Fluorescent Liquid-Crystalline Nanoparticles for Cancer Theranostics. *Langmuir* **2015**, *31*, 9566–9575.
- (9) Biffi, S.; Andolfi, L.; Caltagirone, C.; Garrovo, C.; Falchi, A. M. Lippolis, V.; Lorenzon, A.; Macor, P.; Meli, V.; Monduzzi, M.; Obiols-Rabasa, M.; Petrizza, L.; Prodi, L.; Rosa, A.; Schmidt, J.; Talmon, Y.; Murgia, S. Cubosomes for *in vivo* Fluorescence Lifetime Imaging. *Nanotechnology* **2017**, *28*, 055102.
- (10) Tran, N.; Bye, N.; Moffat, B. A.; Wright, D. K.; Cuddihy, A.; Hinton, T. M.; Hawley, A. M.; Reynolds, N. P.; Waddington, L. J.; Mulet, X.; Turnley, A. M.; Morganti-Kossmann, M. C.; Muir, B. W. Dual-Modality NIRF-MRI Cubosomes and Hexosomes: High Throughput Formulation and *in vivo* Biodistribution. *Mat. Sci. Eng. C* **2017**, *71*, 584–593.
- (11) Karami, Z.; Hamidi, M. Cubosomes: Remarkable Drug Delivery Potential. *Drug Discov. Today* **2016**, *21*, 789–801.
- (12) *Handbook of Polymers for Pharmaceutical Technologies: Structure and Chemistry*, Volume 1, Eds: V.K. Thakur, M.K. Thakur, Wiley 2015.
- (13) *Smart Materials for Tissue Engineering: Fundamental Principles*, Volume 24, Eds: Q. Wang, Royal Society of Chemistry (RSC) 2016.
- (14) Singh, R. P.; Gangadharappa, H. V.; Mruthunjaya, K. Phospholipids: Unique Carriers for Drug Delivery Systems. *J. Drug Deliv. Sci. Technol.* **2017**, *39*, 166–179.
- (15) Li, J.; Wang, X.; Zhang, T.; Wang, C.; Huang, Z.; Luo, X.; Deng, Y. A Review on Phospholipids and Their Main Applications in Drug Delivery Systems. *Asian J. Pharm. Sci.* **2015**, *10*, 81–98.
- (16) McClements, D. J.; Gumus, C. E. Natural Emulsifiers - Biosurfactants, Phospholipids, Biopolymers, and Colloidal Particles: Molecular and Physicochemical Basis of Functional Performance. *Adv. Colloid Interface Sci.* **2016**, *234*, 3–26.

- (17) Pentak, D.; Maciążek-Jurczyk, M. Self-Assembled Nanostructures Formed by Phospholipids and Anticancer Drugs. Serum Albumin-Nanoparticle Interactions. *J. Mol. Liq.* **2016**, *224*, 1–8.
- (18) Rattanapak, T.; Young, K.; Rades, T.; Hook, S. Comparative Study of Liposomes, Transfersomes, Ethosomes and Cubosomes for Transcutaneous Immunisation: Characterisation and *in vitro* Skin Penetration. *J. Pharm. Pharmacol.* **2012**, *64*, 1560–1569.
- (19) Md, S.; Haque, S.; Madheswaran, T.; Zeeshan, F.; Meka, V. S.; Radhakrishnan, A. K.; Kesharwani, P. Lipid Based Nanocarriers System for Topical Delivery of Photosensitizers. *Drug Discov. Today* **2017**, *22*, 1274–1283.
- (20) Balansin Rigon, R.; Oyafuso, M. H.; Fujimura, A. T.; Gonçalez, M. L.; Haddad do Prado, A.; Daflon Gremião, M. P.; Chorilli, M. Nanotechnology-Based Drug Delivery Systems for Melanoma Antitumoral Therapy: A Review. *BioMed Research Int.* **2015**, *2015*, 1–22.
- (21) Kalal, B. S.; Upadhyay, D.; Pai, V. R. Chemotherapy Resistance Mechanisms in Advanced Skin Cancer. *Oncol. Rev.* **2017**, *11*, 326–343.
- (22) Davids, L. M.; Kleeman, B. Combating melanoma: The use of Photodynamic Therapy as a Novel, Adjuvant Therapeutic Tool. *Cancer Treat. Rev.* **2011**, *37*, 465–475.
- (23) Zhao, B.; Yin, J. J.; Bilski, P. J.; Chignell, C. F.; Roberts, J. E.; He, Y. Y. Enhanced Photodynamic Efficacy Towards Melanoma Cells by Encapsulation of Pc4 in Silica Nanoparticles. *Toxicol. Appl. Pharmacol.* **2009**, *241*, 163–172.
- (24) Bazylińska, U.; Frąckowiak, R.; Brzózka, Z.; Wilk, K. A. The Effect of Anionic Dicapalic Surfactants on Fabrication of Varied-Core Nanocarriers for Sustained Release of Porphyrin Photosensitizers. *J. Photochem. Photobiol. B: Biology* **2017**, *166*, 169–179.
- (25) Zhang, D.; Wu, M.; Zeng, Y.; Wu, L.; Wang, Q.; Han, X.; Liu, X.; Liu, J.; Chlorin e6 Conjugated Poly(dopamine) Nanospheres as PDT/PTT Dual-Modal Therapeutic Agents for Enhanced Cancer Therapy. *ACS Appl. Mater. Int.* **2015**, *7*, 8176–8187.

- (26) Bazylińska, U.; Saczko, J. Nanoemulsion-Templated Polyelectrolyte Multifunctional Nanocapsules for DNA Entrapment and Bioimaging. *Colloid Surf. B: Biointerfaces* **2016**, *137*, 191–203.
- (27) Murgia, S.; Falchi, A. M.; Meli, V.; Schillén, K.; Lippolis, V.; Monduzzi, M.; Rosa, A.; Schmidt, J.; Talmon, Y.; Bizzarri, R.; Caltagirone, C. Cubosome Formulations Stabilized by a Dansyl-Conjugated Blockcopolymer for Possible Nanomedicine Applications. *Colloid. Surf. B: Biointerfaces* **2015**, *129*, 87–94.
- (28) Choromańska, A.; Saczko, J.; Kulbacka, J.; Kamińska, I.; Skołucka, N.; Majkowski, M.; Comparison of the Influence of Photodynamic Reaction on the Me45 and MEWO Cell Lines *in vitro*. *Contemp. Oncol. (Pozn)*. **2012**, *16*, 240–243.
- (29) Bazylińska, U.; Wawrzyńczyk, D.; Kulbacka, J.; Frąckowiak, R.; Cichy, B.; Bednarkiewicz, A.; Samoć, M.; Wilk, K. A. Polymeric Nanocapsules with Upconverting Nanocrystals Cargo Make Ideal Fluorescent Bioprobes. *Sci. Rep.* **2016**, *6*, 29746–29760.
- (30) Müller, R. H.; Jacobs, C.; Kayser, O. Nanosuspensions as Particulate Drug Formulations in Therapy. Rationale for Development and What We Can Expect for the Future. *Adv. Drug Deliv. Rev.* **2001**, *47*, 3–19.
- (31) Lu, Y.; Kang, W.; Jiang, J.; Chen, J.; Xu, D.; Zhang, P.; Zhang, L.; Feng, H.; Wu, H. Study on the Stabilization Mechanism of Crude Oil Emulsion with an Amphiphilic Polymer using the b-Cyclodextrin Inclusion Method. *RSC Adv.* **2017**, *7*, 8156–8166.
- (32) Ostolska, I.; Wiśniewska, M. The Impact of Polymer Structure on the Adsorption of Ionic Polyamino Acid Homopolymers and Their Diblock Copolymers on Colloidal Chromium (III) Oxide. *RSC Adv.* **2015**, *5*, 28505–28514.
- (33) Rizwan, S. B.; Assmus, D.; Boehnke, A.; Hanley T.; Boyd, B. J.; Rades, T.; Hook, S. Preparation of Phytantriol Cubosomes by Solvent Precursor Dilution for the Delivery of Protein Vaccines. *Eur. J. Pharm. Biopharm.* **2011**, *79*, 15–22.

- (34) Ramachandran, G. K.; Yeow, C. H. Proton NMR Characterization of Intact Primary and Metastatic Melanoma Cells in 2D & 3D Cultures. *Biol. Research* **2017**, *50*, 12.
- (35) Lopes, L. B.; Collett, J. H.; Bentley, M. V. Topical Delivery of Cyclosporin A: an *in vitro* Study using Monoolein as a Penetration Enhancer. *Eur. J. Pharm. Biopharm.* **2005**, *60* 25–30.
- (36) Carboni, M.; Falchi, A. M. Sinico, C.; Manca, M. L.; Murgia, S.; Lampis, S.; Schmidt, J.; Talmon, Y.; Monduzzi, M. Physicochemical, Cytotoxic, and Dermal Release Features of Novel Cationic Liposome Nanocarrier. *Adv. Healthcare Mater.* **2013**, *2*, 692–701.
- (37) *Drug Delivery Across Physiological Barriers*, Eds: S. Muro, CRC Press Taylor and Francis Group, 2016.
- (38) *Handbook of Biophotonics*, Eds: Wen-Tyng Li, Wiley, 2013; Chapter 23 Nanoparticles for Photodynamic Therapy.

## TABLE OF CONTENTS GRAPHICS



COLLOIDAL STABILIZATION

